한국항해항만학회지 제44권 제2호
J. Navig. Port Res. Vol. 44, No. 2 : 53-64, April 2020 (ISSN:1598-5725(Print)/ISSN:2093-8470(Online))
DOI : http://dx.doi.org/10.5394/KINPR.2020.44.2.53

Analysis on Hydrodynamic Force Acting on a Catamaran at Low Speed Using RANS Numerical Method

Thi Loan Mai · Tien Thua Nguyen** · Myungjun Jeon*** · † Hyeon Kyu Yoon*

,,***Student, Graduate Sschool of Changwon National University, Gyeongsangnam-do, 51140, Korea*
† Professor of Changwon National University, Gyeongsangnam-do, 51140, Korea

Abstract : *This paper discusses the hydrodynamic characteristics of a catamaran at low speed. In this study, the Delft 372 catamaran model was selected as the target hull to analyze the hydrodynamic characteristics by using the RANS (Reynold-Averaged Navier-Stokes) numerical method. First, the turbulence study and mesh independent study were conducted to select the appropriate method for numerical calculation. The numerical method for the CFD (Computational Fluid Dynamic) calculation was verified by comparing the hydrodynamic force with that obtained experimentally at high speed condition and it rendered a good agreement. Second, the virtual captive model test for a catamaran at low speed was conducted using the verified method. The drift test with drift angle 0-180 degrees was performed and the resulting hydrodynamic forces were compared with the trends of other ship types. Also, the pure rotating test and yaw rotating test proposed by Takashina, (1986) were conducted. The Fourier coefficients obtained from the measured hydrodynamic force were compared with those of other ship types. Conversely, pure sway test and pure yaw test also were simulated to obtain added mass coefficients. By analyzing these results, the hydrodynamic coefficients of the catamaran at low speed were estimated. Finally, the maneuvering simulation in low speed conditions was performed by using the estimated hydrodynamic coefficients.*

Key words : *Delft 372 Catamaran, Low Speed, Hydrodynamic Coefficients, RANS Numerical Method, Virtual Captive Model Test, Maneuvering Simulation.*

1. Introduction

Nowadays, catamaran is widely used for variety of purposes due to their excellent performance in terms of safety, resistance performance, transverse stability, and large deck area. The catamaran not only operates at high speed, but it also operates at low speed in special cases such as near harbor. A large number of theoretical and numerical studies as well as experimental investigations have recently been conducted with a focus on the hydrodynamic force acting on the catamaran. For example, Zlatev et al.(2009) performed an experiment involving a high-speed catamaran at Bulgarian Ship Hydrodynamic Center (BSHC) to investigate the maneuvering characteristics at various water depth ratios and different Froude numbers. The results showed that the hydrodynamic force increases with decreasing water depth and increasing Froude number. Milanov et al.(2012) conducted an experiment on a Delft 372 catamaran with the water-jet in both deep and shallow waters. The hydrodynamic coefficients were estimated to predict the maneuverability, and then the mathematical model for the water-jet of Delft 372 catamaran was established. Other studies have also investigated the seakeeping performance (Castiglione et al., 2011), resistance performance, and interaction between demi-hulls (Broglia et al., 2011) for Delft 372 catamaran at high speed. However, the low speed movement of the catamaran near the harbor has yet to be studied.

The ship operates at low speed in such a situation to move slowly and avoid the obstacle. Takashina (1986) proposed the pure rotating test and the yaw rotating test to calculate hydrodynamic coefficients for tugboat at low speed and large drift angle. Fourier series was applied to estimate hydrodynamic coefficients, and a mathematical model is established for ship at low speed condition. In a different study, Umeda et al.(1989) investigated cross flow force and lateral force through a circular motion test of the trawler at low speed and large drift angle. A mathematical model was developed for validation for both a longitudinal symmetric ship and a non-symmetric ship. In addition, Oh et al.(2012) presented a number of models for ship maneuvering at low speed proposed by other researchers. A

† Corresponding author, hkyoon@changwon.ac.kr 055)213-3683
Note) This paper was presented on the subject of "Analysis on Hydrodynamic Force acting on a Catamaran at Low Speed using RANS Numerical Method" in 2019 Joint Conference ANC 2019 proceedings (Busan Port International Exhibition & Convention Center (BPEX), 21st-23rd November, 2019, pp.268-277).

comparison among the models for various types of ship is implemented to help accurately predict the hydrodynamic force of any given ship in low speed.

Regarding the use of CFD-based simulation to estimate hydrodynamic characteristics, Hajivand et al.(2015) have performed a virtual captive model test for DTMB 5512 using RANS (Reynolds-Averaged Navier-Stokes) numerical method based on STAR-CCM+ to estimate the hydrodynamic characteristics. OpenFOAM software has also been used to predict hydrodynamic characteristics for KCS by Islam et al.(2018). In addition, Liu et al.(2018) conducted a virtual captive model test for KCS (KRISO Container Ship) by using unsteady RANS to predict linear and nonlinear hydrodynamic coefficients in the 3rd-order Abkowiz model. The uncertainty analysis for GCI (Grid Convergence Index) and time step is conducted for dynamic testing, and the standard turning and zigzag maneuvers are predicted by using the estimated hydrodynamic coefficients. The conditions used in these studies included a conventional ship and a small or moderate drift angle.

This paper focuses on estimating the hydrodynamic force acting on Delft 372 catamaran operating at low speed by using RANS-based solver in Ansys FLUENT 17.2. A verification is performed for RANS-based method with the turbulence study and mesh independence study to select the most appropriate method. A virtual captive model test is simulated to predict hydrodynamic force at low speed. Especially, large drift angle is performed in the static drift test, pure rotating test, and yaw rotating test at low speed. Fourier approximation is applied to estimate hydrodynamic coefficients by analyzing the calculated hydrodynamic force. The trajectory of the catamaran at low speed is predicted using estimated hydrodynamic coefficient.

2. Theory Background

2.1 Coordinate system

Two coordinate systems are used to define the kinematic and hydrodynamic forces acting on the Delft 372 catamaran. Fig. 1 shows the earth-fixed coordinate system Ox_0y_0 that is set to be fixed with origin and the body-fixed coordinate system Oxy that is fixed with the ship hull. Both the coordinate systems follow the right-hand rule, which means that the vertical axes are pointing downward and the lateral axes are pointing to the right-hand side. The origin of body-fixed coordinate system is located at the midship and its x-axis is directed to ship bow. The motion equation for a surface ship in a horizontal plane is as follows,

$$m\left(\dot{u}-vr-x_G r^2\right)=X \tag{1}$$

$$m\left(\dot{v}+ur+x_G\dot{r}\right)=Y$$

$$I_z\dot{r}-mx_G\left(\dot{v}+ur\right)=N$$

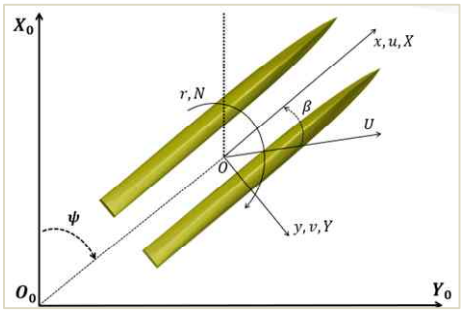

Fig. 1 Coordinate system

where m is the ship mass, u, v and r are the surge velocity, sway velocity, and yaw rate, respectively. In addition, $\dot{u}$, $\dot{v}$, and $\dot{r}$ are the corresponding surge acceleration, sway acceleration, and angular acceleration, respectively. I_z is the moment of inertia about the z-axis. X and Y are the resultant forces acting on ship in surge and sway direction, respectively. N indicates the resultant moment in the yaw direction. U and β indicate the ship speed and drift angle.

2.2 Governing equation

In this study, the flow around the ship is assumed to be incompressible. The continuity equation and Navier-Stokes equation are chosen as governing equations:

$$\frac{\partial \overline{u_i}}{\partial x_i}=0 \tag{2}$$

$$\frac{\partial \overline{u_i}}{\partial t}+u_j\frac{\partial \overline{u_i}}{\partial x_j}=-\frac{1}{\rho}\frac{\partial p}{\partial x_i}+\nu\frac{\partial^2 \overline{u_i}}{\partial x_i \partial x_j}-\frac{\partial \tau_{ij}}{\partial x_j}+\overline{f_i} \tag{3}$$

where u_i and u_j are the average velocity components; u'_i and u'_j are the fluctuating components; p is the average pressure; ν is the kinematic viscosity; x_i and x_j are the i^{th} and j^{th} coordinates in the fluid domain respectively; and ρ is the water density.

2.3 Dimensionless quantity

The obtained force and moment from simulation are

non-dimensionalized by length (L), draft (T), and speed. The non-dimensionless force, moment, and motion are given as follows,

$$X' = \frac{X}{0.5\rho U^2 LT}, Y' = \frac{Y}{0.5\rho U^2 LT}, N' = \frac{N}{0.5\rho U^2 L^2 T} \quad (4)$$

$$u' = \frac{u}{U}, v' = \frac{v}{U}, r' = \frac{rL}{U} \quad (5)$$

2.4 CFD-Based modeling

2.4.1 Numerical modeling

The rectangular domain covering the catamaran is generated to simulate the virtual captive model test. The computational domain is selected to be sufficiently large to avoid backflow and side flow at a high drift angle. In the static test, the dimension of the rectangular is 7L in length, 4L in width, and 2.5L in height. The rectangular is also covered for the inner domain. In the dynamic test, the dimensions are 6L, 4L, and 2.5L for the length, width, and height of the rectangular, respectively. The inner domain is covered a cylinder with a radius of 2.5 m and a height of 1 m to avoid mesh failure at sharp corners. In addition, a physical condition is applied to the boundaries domain. The inlet boundary condition upstream is taken as a pressure-inlet with an open channel; the outlet condition downstream is taken as a pressure-outlet with an open channel. A no-slip wall is set for the hull face and symmetry is assigned for the top face, bottom face, and side faces. The Volume of Fluid is applied to model the two-phase volume of the fluid technique. The fluid domain is discretized into a tetrahedral unstructured mesh in the inner domain of the static test and the whole domain of dynamic test. Furthermore, a hexahedron structured with multi-block is generated in the outer domain of the static test in order to reduce the number of elements. Because the wall function is applied to improve the accuracy of the flow resolution, prism layer mesh is used near the hull surface to resolve the boundary layer flow. The y+ value of 30 is estimated for Reynolds number of 9.7E+5. The mesh generation for the static test and the dynamic test is shown in Fig. 2.

According to Practical Guidelines for ship CFD Application (ITTC, 2011), a two-equation turbulence model is used to enable an accurate prediction of the ship dynamic. The turbulence models of k-ε Realizable and k-ω SST (Shear Stress Transport) are employed in the calculation. In addition, the SIMPLE (Semi-implicit Method for Pressure Link Equations) algorithm is applied to obtain the pressure and velocity field. The quantities at the cell faces are calculated from the cell centered values using the second order upwind method.

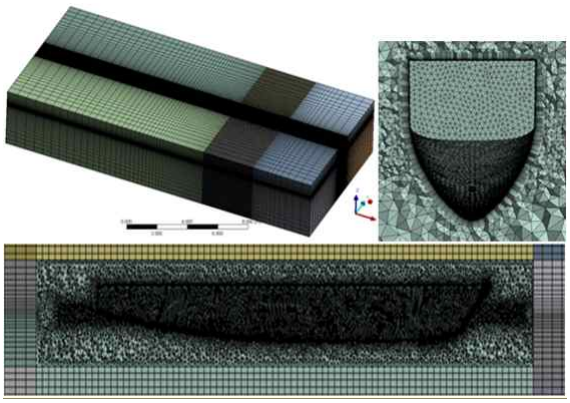

a) Static test

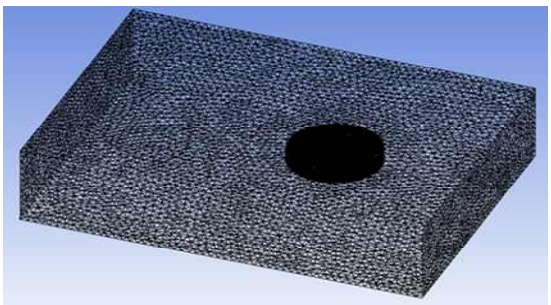

b) Dynamic test

Fig. 2 Mesh generation

2.4.2 Numerical analysis

Before proceeding with the computation, it is necessary to first perform a verification study. Thus, the turbulence study and mesh independence study are conducted to select the most appropriate method for this study. Experimental results obtained from the BSHC (Bulgarian Ship Hydrodynamic Center) are used for verification in the present study.

In the turbulence study, two turbulence models of k-ε Realizable and k-ω SST are evaluated initially. A drift test case of 6 degrees is carried out at the Froude number of 0.3 for two turbulence model to obtain the hydrodynamic force.

For the mesh independence study, three different grid size are used and the corresponding forces are evaluated in a drift test with a drift angle of 6 degrees at Froude number 0.3. The grid refinement is achieved by applying a refinement factor $r_G = \sqrt{2}$ to the base size. The Grid Convergence Index (GCI) method is applied to evaluate the

discretization error of the calculation method. Using this method, the grid densities of fine mesh, medium mesh, and coarse mesh is prepared by changing the base size with a refinement factor. The grid parameter is expressed in Eq. (6) and the GCI is defined as Eq. (7).

$$p = \frac{1}{\ln(r_G)} \left| \ln \left| \frac{\epsilon_{32}}{\epsilon_{21}} \right| \right| \tag{6}$$

$$GCI_{ij}^{fine} = \frac{1.25 e_{ij}}{r^p - 1} \tag{7}$$

where $\epsilon_{ij} = \phi_i - \phi_j$, and ϕ indicate the solutions with fine, medium, and coarse input parameters. $e_{ij} = |(\phi_j - \phi_i)/\phi_j|$ is the approximate relative error.

2.5 Captive model test

2.5.1 Static drift test

The ship is towed at a constant speed with a constant drift angle ranging from zero to 180 degrees. Fig. 3 shows a schematic of this motion.

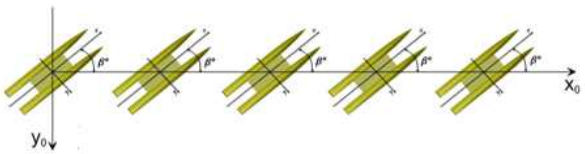

Fig. 3 Static drift test

Fourier approximation is used in deriving the hydrodynamic coefficients. The following expression using Fourier series is expressed as follows,

$$Y', N' = \sum_{k=1}^{k} S_k \sin k\beta \tag{8}$$

2.5.2 Pure rotating test

The test is conducted with a ship speed of zero while rotating around a vertical axis through the center of gravity of the ship with a constant yaw rate, as shown in Fig. 4. The hydrodynamic force in the pure rotating test is given in Eq. (9) as:

$$X_H = 0,\ Y_H \approx 0 \tag{9}$$

$$N_H = N'_{r|r|} r'|r'| \times \frac{1}{2} \rho L^4 T$$

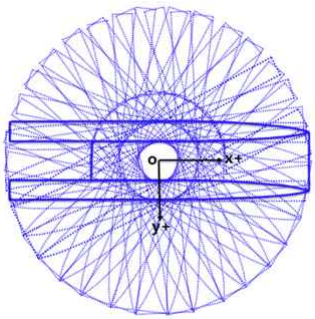

Fig. 4 Pure rotating test

2.5.3 Yaw rotating test

As shown in Fig. 5, the ship is simulated to rotate around the vertical axis through the center of gravity at a constant speed and a constant yaw rate. The motion given to the ship during the yaw rotating test with a large drift angle can be described as follows,

$$\beta = rt,\ u = U\cos\beta,\ v = -Ur\sin\beta \tag{10}$$

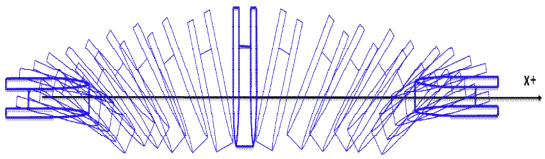

Fig. 5 Yaw rotating test

The hydrodynamic force for the drift angle measured between zero degrees and 360 degrees is described as the sine and cosine functions. Thus, the hydrodynamic force can be expressed in terms of Fourier approximation with respect to the drift angle in Eq. (11). On the other hand, the variations of these coefficients are supposed as shown in Eq. (12).

$$X_H, Y_H, N_H = \sum_{k=0}^{K} \left(S_k^{X,Y,N} \sin k\beta + C_k^{X,Y,N} \cos k\beta \right) \tag{11}$$

$$S_k^X = S_{k1} r' + S_{k2} r'|r'| \qquad C_k^X = C_{k0} + C_{k1}|r'| + C_{k2} r'^2$$

$$S_k^{Y,N} = S_{k0} + S_{k1}|r'| + S_{k2} r'^2 \qquad C_k^{Y,N} = C_{k1} r' + C_{k2} r'|r'| \tag{12}$$

By substituting Eq. (12) into Eq. (11), X', Y' and N' can be expressed as shown in Eqs. (13)-(15), respectively.

$$X'_H = C_{10}\cos\beta + S_{11} r' \sin\beta \tag{13}$$

$$Y'_H=(S_{10}+S_{11}|r'|)\sin\beta+(S_{30}+S_{31}|r'|)\sin3\beta \quad (14)$$
$$+(S_{50}+S_{51}|r'|)\sin5\beta+(C_{11}r'+C_{12}r'|r'|)\cos\beta$$
$$+(C_{31}r'+C_{32}r'|r'|)\cos3\beta$$

$$N'_H=(S_{10})\sin\beta+(S_{20}+S_{21}|r'|)\sin2\beta+(S_{30})\sin3\beta \quad (15)$$
$$+(S_{40}+S_{41}|r'|)\sin4\beta+(C_{21}r'+C_{22}r'|r'|)\cos2\beta$$

On the other hand, the terms of the Fourier coefficients can be transformed into conventional expressions with hydrodynamic coefficients according to the relationship between β and u, and v based on trigonometry. According to the mathematical model proposed by Takashina (1986), the hydrodynamic equations for X', Y', and N' are respectively expressed as follows,

$$X'_H=X'_{uu}u'^2+X'_{vr}v'r' \quad (16)$$

$$Y'_H=Y'_v v'+Y'_{vvv}v'^3+Y'_{vvvvv}v'^5+Y'_{ur}u'r' \quad (17)$$
$$+Y'_{v|r|}v'|r'|+Y'_{ur|r|}u'r'|r'|$$

$$N'_H=N'_v v'+N'_{uv}u'v'+N'_{vvv}v'^3+N'_{uvvv}uv'^3+N'_r r' \quad (18)$$
$$+N'_{r|r|}r'|r'|+N'_{uv|r|}u'v'|r'|+N'_{vv|r|}v'^2|r|$$

Finally, the hydrodynamic coefficients for X', Y', and N' can be respectively obtained from the following relationships shown in Eqs. (19)~(21).

$$X'_{uu}=C_{10},\quad X'_{vr}=-S_{11} \quad (19)$$

$$Y'_v=-S_{10}-3S_{30}-5S_{50}\quad Y'_{v|r|}=-S_{11}-3S_{31}-5S_{51} \quad (20)$$
$$Y'_{vvv}=4S_{30}+20S_{50}\quad Y'_{ur}=C_{11}-3C_{31}$$
$$Y'_{vvvvv}=-16S_{50}\quad Y'_{ur|r|}=C_{12}-3C_{32}$$

$$N'_v=-S_{10}-3S_{30}\quad N'_r=C_{21} \quad (21)$$
$$N'_{uv}=-2S_{20}-4S_{40}\quad N'_{r|r|}=C_{22}$$
$$N'_{vvv}=4S_{30}\quad N'_{uv|r|}=-2S_{21}-4S_{41}$$
$$N'_{uvvv}=8S_{40}\quad N'_{vv|r|}=-2C_{21}$$

It should be noted that X'_{uu} is given as a function of velocity based on the resistance results.

2.5.4 Harmonic test

The ship is simulated to oscillate in a sinusoidal motion at a constant speed and a constant frequency. The pure sway test and the pure yaw test are achieved in this study. The main reason these tests are performed is to estimate the added mass coefficients with v oscillating harmonically in the pure sway test and the coefficients relative to the yaw rate with harmonic oscillating yaw motion in the pure yaw test. The motions of the pure sway test and the pure yaw test is described in Eqs. (22) and (23), respectively. Figs. 6~7 show the definitions of the pure sway test and the pure yaw test, respectively.

$$y=-y_{\max}\sin\omega t \quad (22)$$
$$v=-y_{\max}\omega\cos\omega t$$
$$\dot{v}=y_{\max}\omega^2\sin\omega t$$

$$\psi=-\psi_{\max}\cos\omega t \quad (23)$$
$$r=\psi_{\max}\omega\sin\omega t$$
$$\dot{r}=\psi_{\max}\omega^2\cos\omega t$$

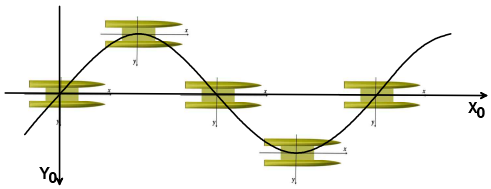

Fig. 6 Pure sway test

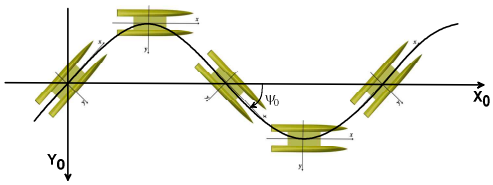

Fig. 7 Pure yaw test

The mathematical models for the harmonic test (Hajivand et. al., 2015 and Liu et. al., 2018) are shown in Eqs. (24) and (25) for pure sway test and pure yaw test, respectively.

$$X=X_{vv}v^2 \quad (24)$$
$$Y=Y_{\dot{v}}\dot{v}+Y_v v+Y_{vvv}v^3$$
$$N=N_{\dot{v}}\dot{v}+N_v v+N_{vvv}v^3$$
$$X=X_{rr}r^2 \quad (25)$$
$$Y=Y_{\dot{r}}\dot{r}+Y_r r+Y_{rrr}r^3$$
$$N=N_{\dot{r}}\dot{r}+N_r r+N_{rrr}r^3$$

Fourier approximation for the harmonic test is adopted to derive the hydrodynamic coefficients. The harmonic forms of the pure sway test and the pure yaw test are achieved

by substituting the motion into the mathematical model as presented in Eqs. (26) and (27) for pure sway and pure yaw, respectively.

$$X = X_0 + X_{c2}\cos 2\omega t \tag{26}$$

$$Y = Y_{c1}\cos\omega t + Y_{s1}\sin\omega t + Y_{s3}\cos 3\omega t$$

$$N = N_{c1}\cos\omega t + N_{s1}\sin\omega t + N_{s3}\cos 3\omega t$$

$$X = X_0 + X_{c2}\cos 2\omega t \tag{27}$$

$$Y = Y_{s1}\sin\omega t + Y_{c1}\cos\omega t + Y_{s3}\sin 3\omega t$$

$$N = N_{s1}\sin\omega t + N_{c1}\cos\omega t + N_{s3}\sin 3\omega t$$

The Fourier sine and cosine coefficients in these expressions are given in Table 1. The functions of the N component are not listed in the table since they are the same as those of the Y component, and it can be obtained by replacing "Y" with "N".

Table 1 Fourier coefficients for harmonic test

	X component	Y component
Pure sway	$X_0 = \frac{1}{2}X_{vv}v_{\max}^2$ $X_{c2} = \frac{1}{2}X_{vv}v_{\max}^2$	$Y_{c1} = -\left(Y_v v_{\max} + \frac{3}{4}Y_{vvv}v_{\max}^3\right)$ $Y_{s1} = Y_{\dot{v}}\dot{v}_{\max}$ $Y_{c3} = -\frac{1}{4}Y_{vvv}v_{\max}^3$
Pure yaw	$X_0 = \frac{1}{2}X_{rr}r_{\max}^2$ $X_{c2} = -\frac{1}{2}X_{rr}r_{\max}^2$	$Y_{s1} = -\left(Y_r r_{\max} + \frac{3}{4}Y_{rrr}r_{\max}^3\right)$ $Y_{c1} = Y_{\dot{r}}\dot{r}_{\max}$ $Y_{s3} = -\frac{1}{4}Y_{rrr}r_{\max}^3$

3. Results

3.1 Case study

The target ship in this study is the Delft 372 catamaran model that originally used in TU-Delft by Vant Veer (1988). Main parameters of the catamaran are listed in Table 2. Fig. 16 shows the 3D model of Delft 372 catamaran.

Table 2 Main parameters of Delft 372 catamaran

Main particulars	Full scale	Model scale
Scale	1.00	33.33
Length between perpendiculars, L_{PP} (m)	100.00	3.00
Beam overall, B_{OA} (m)	31.33	0.94
Beam demi-hull, b (m)	8.00	0.24
Distance between center of the demi-hull, H (m)	23.33	0.70
Separation distance, s (m)	15.33	0.46
Draft, T (m)	5.00	0.15

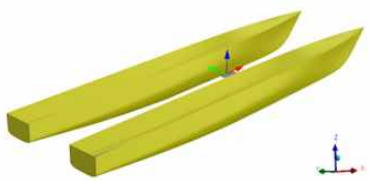

Fig. 8 Delft 372 catamaran

The computational conditions are depicted in Table 3 for static test and Table 4 for dynamic test.

Table 3 Static test

Test	Fr (-)	$\beta(^\circ)$	
Static drift	0.06	0~180	0~18, interval 3 20~160 interval 10 162~180, interval 3

Table 4 Dynamic test

Test	Fr (-)	r (rad/s)	v (m/s)
Pure rotating	0	0.105, 0.140, 0.175, 0.209	-
Yaw rotating	0.06, 0.12	0.070, 0.105, 0.140, 0.175, 0.209	-
Pure sway	0.06	-	0.027, 0.032, 0.038, 0.043
Pure yaw	0.06	0.045, 0.052, 0.058, 0.065	-

3.2 CFD verification

3.2.1 Turbulence study

Fig. 9 shows the comparison of the turbulence study results. It can be seen that both of the turbulence models predict the hydrodynamic force of the catamaran with good accuracy. However, the results of the k-ω SST turbulence model are slightly better than those of the other two.

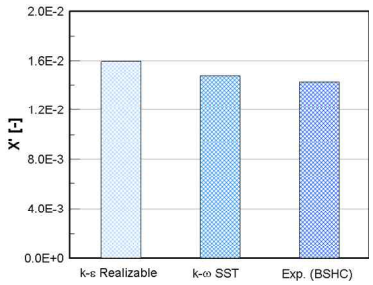

a) Surge force

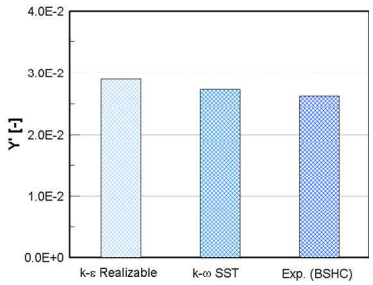

b) Sway force

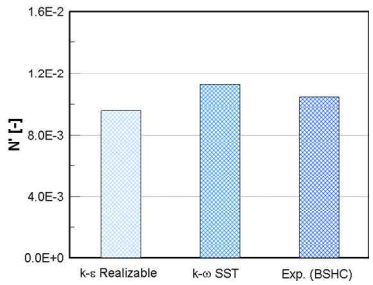

c) Yaw moment

Fig. 9 Comparison of turbulence study

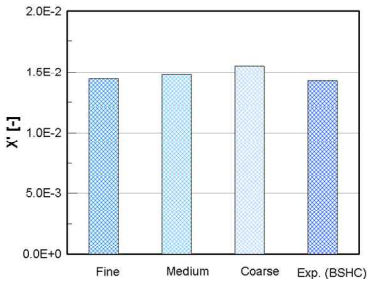

a) Surge force

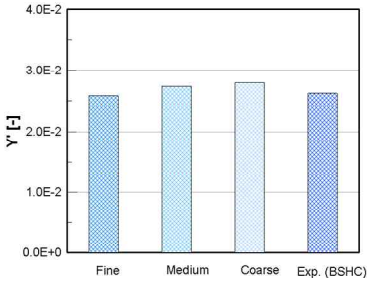

b) Sway force

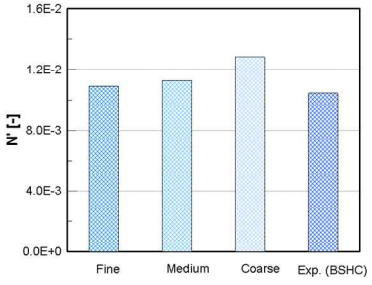

c) Yaw moment

Fig. 10 Comparison of mesh independence study

3.2.2 Mesh independence study

The three densities of the fine grid, the medium grid, and the coarse grid are counted to be approximately 6.77M, 4.90M, and 3.55M, respectively. The mesh independence study is performed with the k-ω SST turbulence model. Table 5 shows the solution of the mesh convergence study. In addition, the computation results obtained from the different mesh sizes are shown in Fig. 10. It indicates that the error of the solution is reduced as the generated grid becomes finer.

Table 5 Estimated convergence ratio

Item	X′	Y′	N′
p	2.24	2.71	2.89
GCI_{fine}	2.47%	4.76%	3.85%

3.2.3 Verification

The verification is simulated for a fine grid with the k-ω SST turbulence model at a Froude number of 0.3 in the case of the drift test. In Fig. 11, the calculated hydrodynamic force is compared with the experimental results from BSHC. It can be seen that the hydrodynamic force of computation results are consistent with the experimental results. Therefore, fine grid and k-ω SST are simulated in further study.

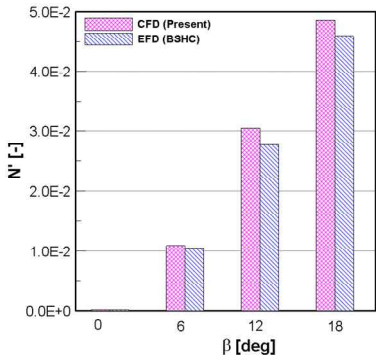

a) Surge force

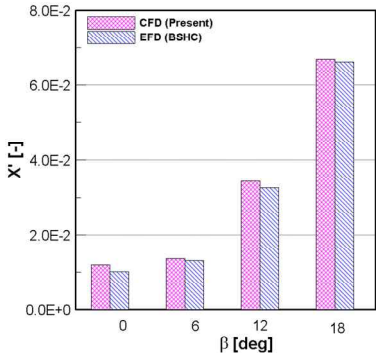

b) Sway force

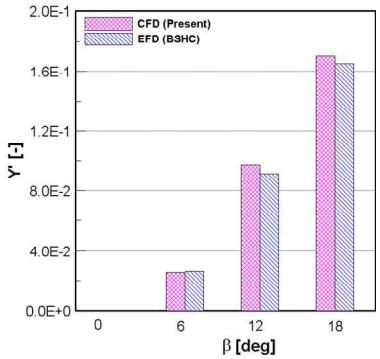

c) Yaw moment

Fig. 11 Comparison of hydrodynamic forces at high speed

3.3 Results of virtual captive model test

3.3.1 Static drift test

The hydrodynamic forces of the static drift test for drift angles ranging from zero to 180 degrees at low speed are shown in Fig. 12. The comparison with other ship types shows that the trend of the hydrodynamic force in the present study is consistent with the trends of the experimental results of the other ship types. However, the difference among results due to the different ship types is observed, especially tugboats. Furthermore, slender shape of a catamaran and slender body ship gives a similar results.

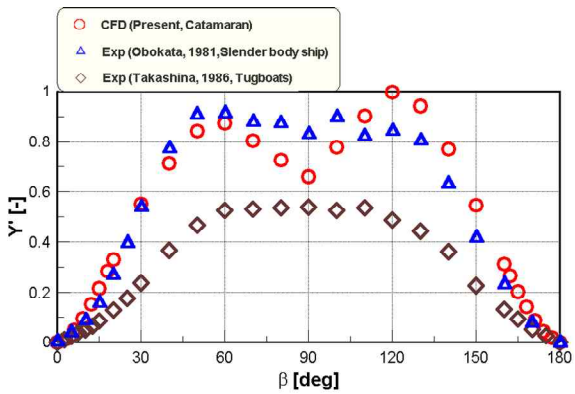

a) Sway force

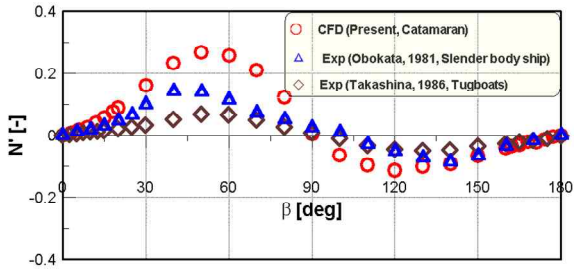

a) Yaw moment

Fig. 12 Hydrodynamic force of the drift test

By approximating the measured data, the Fourier coefficients are obtained by using Eq. (8) and presented in Table 6.

Table 6 Fourier coefficients of the drift test

Fourier coefficients	Sway force (Y′)	Yaw moment (N′)
S_{10}	0.969	0.085
S_{20}	-	0.173
S_{30}	0.133	0.029
S_{40}	-	-0.045
S_{50}	-0.122	-

Furthermore, the below figure shows the velocity contour of static drift test at 90 degrees. It can be seen that the velocity between two side faces where symmetry condition is set. It is nearly same value with inlet velocity despite of low speed condition. Since velocity changes occur around the ship, applying symmetry conditions seems appropriate.

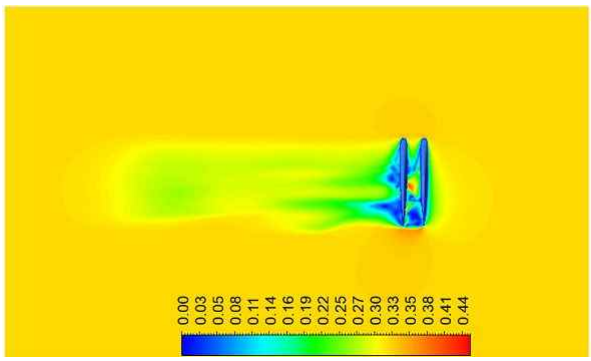

Fig. 13 Velocity contour at 90 degrees

3.3.2 Pure rotating test

Fig. 14 shows the yaw moment acting on the catamaran against the yaw rate squared r|r|. The hydrodynamic coefficient N'r|r| can be obtained based on the ratio of yaw moment to yaw rate squared.

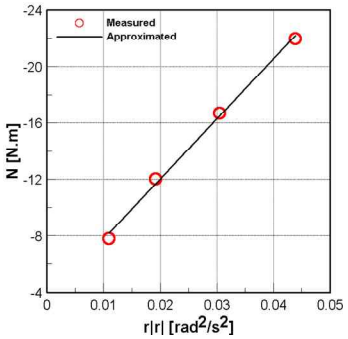

Fig. 14 Yaw moment on hull versus r|r|

3.3.3 Yaw rotating test

The Fourier coefficients obtained from yaw rotating test are plotted against the non-dimensional yaw rates in Figs. 15~17 for X', Y', and N', respectively. In addition, the trends of the Fourier coefficients of catamaran are compared with those of the Fourier coefficients of tugboats obtained by Takashina(1986). It can be observed that Fourier coefficients of the tugboats are smaller than the catamaran results due to the smaller values of hydrodynamic forces of the tugboats as shown in Fig. 12. Nevertheless, the similar trends between tugboats and catamaran can illustrate that the obtained coefficients of catamaran are appropriate results.

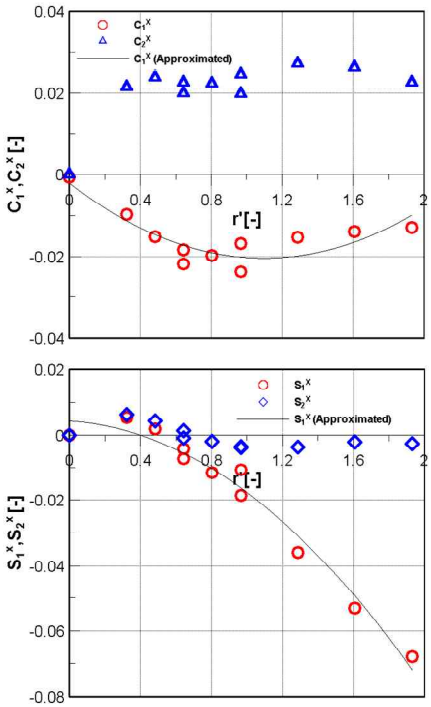

Fig. 15 Fourier coefficients of surge force versus yaw rate

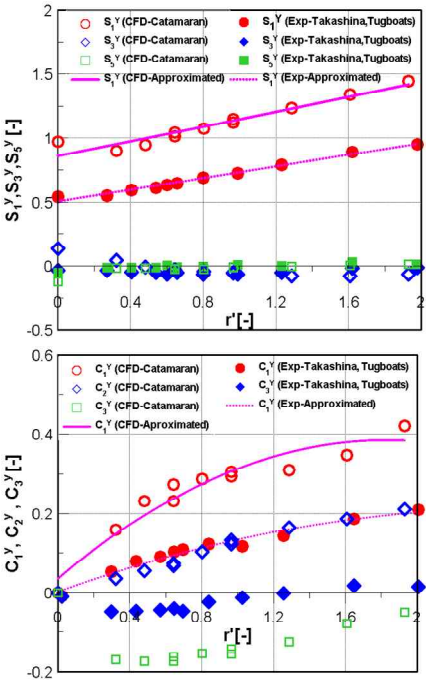

Fig. 16 Fourier coefficients of sway force versus yaw rate

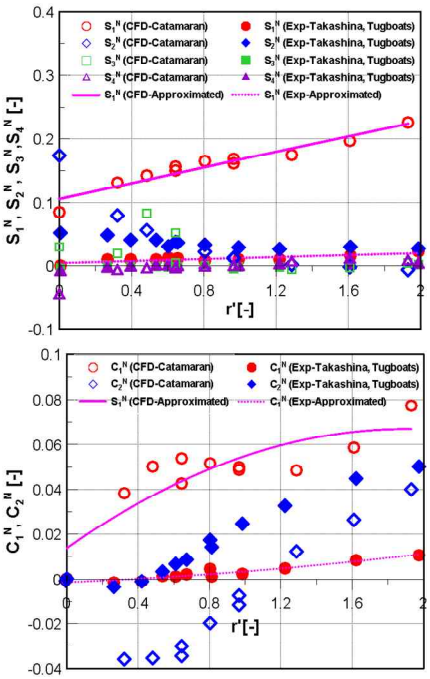

Fig. 17 Fourier coefficients of yaw moment versus yaw rate

3.3.4 Harmonic test

The Fourier coefficients obtained from the harmonic test for in-phase components are drawn versus lateral acceleration in Fig. 18 for the pure sway test and versus yaw rate in Fig. 19 for the pure yaw test. By fitting the in-phase components, the added mass coefficients can be estimated.

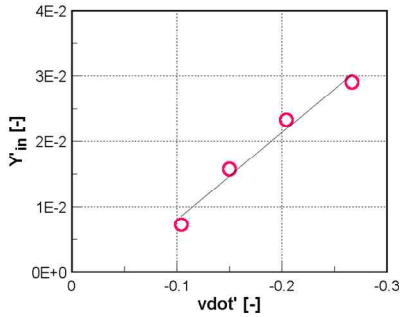

a) Sway force

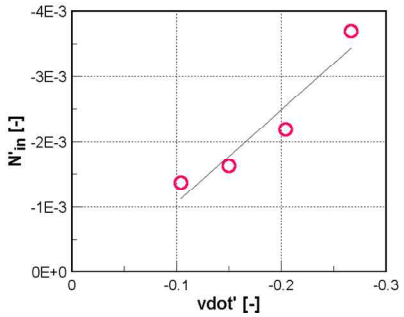

b) Yaw moment

Fig. 18 Fitting in-phase values of sway force and yaw moment versus lateral acceleration

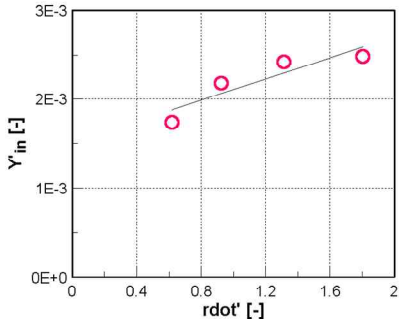

a) Sway force

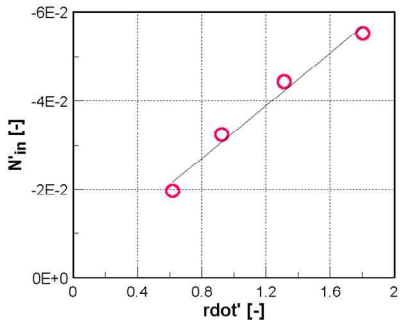

b) Yaw moment

Fig. 19 Fitting in-phase values of sway force and yaw moment versus yaw rate

Finally, the hydrodynamic coefficients of a Delft 372 catamaran operating at low speed are estimated using the virtual captive model test and the results are presented in Table 7.

Table 7 Estimated hydrodynamic coefficients for Delft 372 catamaran at low speed

Coefficient	Values	Coefficient	Values
X'_{uu}	-2.12E-02	N'_{v}	-1.72E-01
X'_{vr}	3.26E-03	N'_{uv}	-1.63E-01
Y'_{v}	-7.60E-01	N'_{vvv}	1.17E-01
Y'_{vvv}	-1.9E+00	N'_{uvvv}	-3.67E-01
Y'_{vvvvv}	1.94E+00	N'_{r}	-4.05E-02
Y'_{ur}	-6.37E-01	$N'_{r\|r\|}$	-8.10E-2
$Y'_{ur\|r\|}$	1.15E+00	$N'_{uv\|r\|}$	2.20E-01
$Y'_{v\|r\|}$	-5.22E-01	N'_{vvr}	8.10E-02
$Y'_{\dot{v}}$	-1.33E-01	$N'_{\dot{v}}$	1.42E-02
$Y'_{\dot{r}}$	6.07E-04	$N'_{\dot{r}}$	-2.96E-02

3.3.5 Maneuvering simulation

The water-jet propulsion is used as propulsor device and steering device. Thus, the right-hand side of Eq. (1) is expressed as

$$X = X_H + X_{WJ} \tag{28}$$

$$Y = Y_H + Y_{WJ}$$

$$N = N_H + N_{WJ}$$

subscript H and WJ indicate hull and water-jet, respectively.

A experiment for Delft 372 catamaran with water-jet propulsion was performed by Milanov, et al., (2012) in order to obtained mathematical model and hydrodynamic coefficients of water-jet as shown in Table 8.

Table 8 Hydrodynamic coefficients of water-jet (Milanov, et al., 2012)

Coefficient	Values	Coefficient	Values
X'_{η}	-2.06E-3	Y'_{δ}	5.30E-4
$X'_{\eta\eta}$	6.04E-3	$Y'_{\delta\eta}$	-4.80E-3
$X'_{\eta\eta\eta}$	-2.40E-3	$Y'_{\delta\eta\eta}$	1.26E-3
$X'_{\delta\delta}$	-1.50E-3	N'_{δ}	-4.50E-4
$X'_{\delta\delta\eta}$	1.12E-2	$N'_{\delta\eta}$	1.68E-3
$X'_{\delta\delta\delta\delta}$	1.74E-2	$N'_{\delta\eta\eta}$	-1.20E-4
$X'_{\delta\delta\delta\delta\eta}$	-7.91E-2		

Fig. 20 shows the simulation result of turning circle maneuvers at low speed when the water-jet impeller RPM is kept to be constant and water-jet nozzle deflection is 35 degrees. The trajectory is described for the turning path. The speed and yaw rate are changing throughout turning circle simulation.

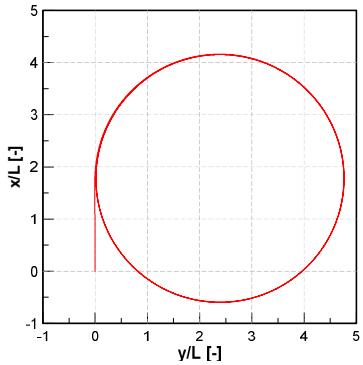

a) Trajectory

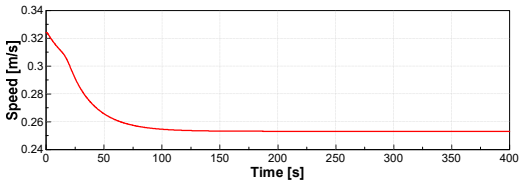

b) Speed

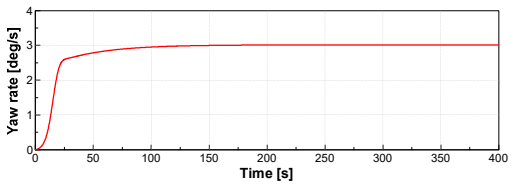

b) Yaw rate

Fig. 20 Turning circle towards the starboard

4. Conclusion

In this study, the virtual captive model test had been implemented using the CFD-based method. Ansys FLUENT version 17.2 was used to simulate the fluid flow through the Delft 372 catamaran. The hydrodynamic force acting on the catamaran at low speed and high drift angle is also estimated.

The results verified that the RANS-based method provided an accurate prediction of the catamaran. The k-ω SST turbulence model and fine mesh were consistent with the experiment results in the case of a drift test at high speed.

CFD simulations were performed for the static drift test, the pure rotating test, the yaw rotating test, and the harmonic test. In particularly, the coupling coefficients for a catamaran at low speed were estimated by performing the pure rotating test and the yaw rotating test. The Fourier approximation provides an accurate prediction of the hydrodynamic coefficients. On the other hand, the obtained hydrodynamic force could be approximated well by the linear reaction with sway velocity, but the added mass coefficients were not fitted very well to the force and moment in the harmonic test. In total, 20 maneuvering coefficients were estimated.

The estimated hydrodynamic coefficients was used to evaluate the catamaran's turning ability at low speed.

Acknowledgements

This work was supported by a grant-in-aid of HANWHA SYSTEMS.

References

[1] 26th International Towing Tank Conference(ITTC) Maneuvering Committee, Proceedings of 26th ITTC.

[2] Broglia, R., Bouscasse, B., Jacob, B., Olivieri, A., Zaghi, S. and Stern, F.(2011), "Calm Water and Seakeeping Investigation for a Fast Catamaran", 11th International Conference on Fast Sea Transportation FAST 2011, pp. 336-344.

[3] Castiglione, T., Stern, F., Bova, S. and Kandasamy, M.(2011), "Numerical investigation of the seakeeping behavior of a catamaran advancing in regular head waves", Ocean Engineering, Vol. 38, No. 16, pp. 1806-1822.

[4] Dogant, T. K.(2013) "URANS and DES for Delft Catamaran for Static Drift Condition in Deep Water", Master Thesis.

[5] Hajivand, A. and Mousavizadegan, S. H.(2015), "Virtual simulation of maneuvering captive tests for a surface vessel", International Journal of Naval Architecture and Ocean Engineering, Vol.7, No. 5, pp. 848-872.

[6] International Towing Tank Conference(ITTC), 2011: ITTC-Recommended Procedures and Guidelines: Practical Guidelines for Ship CFD Applications.

[7] International Towing Tank Conference(ITTC), 2014: ITTC-Recommended Procedures and Guidelines: Captive Model Test Procedures.

[8] Islam, H. and Soares, C. G.(2018), "Estimation of hydrodynamic derivatives of a container ship using PMM simulation in OpenFOAM", Ocean Engineering, Vol. 164, No. 15, pp. 414-425.

[9] Jeon, M. J., Yoon, H. K., Hwang, J. H. and Cho, H. J.(2017), "Analysis of the dynamic characteristics for the change of design parameters of an underwater

vehicle using sensitivity analysis", International Journal of Naval Architecture and Ocean Engineering, Vol. 10, No. 4, pp. 508-519.

[10] Kang, D. H. and Hasegawa, K.(2007), "Prediction method of hydrodynamic forces acting on the hull of a blunt-body ship in the even keel condition", Journal of Marine Science and Technology, Vol. 12, No. 1, pp. 1-14.

[11] Karasuno, K., Matsuno, J., Ito, T. and Igarashi, K.(1992), "A new Mathematical Model of Hydrodynamic Forces and Moment Acting on a Hull during Maneuvering Motion that Occurs under Conditions of Slow Speed and Large Turns", Journal of the Kansai Society of Naval Architects, Japan, No. 217, pp. 125-135.

[12] Liu, Y., Zou, L., Zou, Z. and Guo, H.(2018), "Prediction of ship maneuverability based on virtual captive model tests", Engineering Application of Computation Fluid Mechanics, Vol. 12, No. 1, pp. 334-353.

[13] Milanov, E., Chotukova, V. and Stern, F.(2012), "System Based Simulation of Delft372 Catamaran Maneuvering Characteristics as Function of Water Depth and Approach Speed", 29th Symposium on Naval Hydrodynamics Gothenburg, pp. 26-31.

[14] Nguyen, T. T., Yoon, H. K., Park, Y. B. and Park, C. J.(2018), "Estimation of Hydrodynamic Derivatives of Full-Scale Submarine using RANS Solver", Journal of Ocean Engineering and Technology, Vol. 32, No. 5, pp. 386-392.

[15] Oh, K. G. and Hasegawa, K.(2012), "Ship Maneuvering Hydrodynamic Forces and Moment in Low Speed", Proceedings of 5th PAAMES and AMEC2012, pp. 10-12.

[16] Shenoi, R. R., Krishnankutty, P. and Selvam, R. P.(2016), "Study of Maneuverability of Container Ship with Nonlinear and Roll-Coupled Effects by Numerical Simulations using RANSE-Based Solver", Journal of Offshore Mechanics and Arctic Engineering, Vol. 138, No. 4, pp. 1-14.

[17] Takashina, J.(1986), "Ship Maneuvering Motion due to Tugboats and Its Mathematical Model", the Society of Naval Architects of Japan, Vol. 160, pp. 93-104.

[18] Umeda, N. and Yamakoshi, Y.(1989), "Hydrodynamic Forces acting on a Longitudinally Non-symmetric Ship Under Maneuvering at Low Speed (in Japanese)", Journal of the Kansai Society of Naval Architects, Vol. 211, pp. 127-137.

[19] Zlatev, Z., Milanov, E., Chotukova, N. K. and Stern, F.(2009), "Combined Model-Scale CFD Investigation of the Maneuvering Characteristics of High Speed Catamaran", 10th International Conference on Fast Sea Transportation FAST 2009, pp. 449-462.

Received 19 December 2019
Revised 20 February 2020
Accepted 28 February 2020